XMM-Newton CCF Release Note

XMM-CCF-REL-283

EPIC-pn spatial CTI correction

K. Dennerl & R. Saxton

May 24, 2012

1 CCF components

Name of CCF	VALDATE	List of Blocks changed	Change in CAL HB
EPN_CTI_0024.CCF	2000-01-01	SPATIAL_CTI	YES

2 Change

This change introduces a set of parameters which model the variation of CTI over the EPIC-pn CCDs on a pixel-by-pixel basis. This spatial CTI correction should be applied after all of the other mode-dependent, rate-dependent CTI adjustments have been made and is itself dependent on the observing mode.

3 Scientific impact of this update

`EPN_CTI_0024.CCF` in combination with the task `epspatialcti` improves for the FF and eFF mode the spatial homogeneity of the absolute energy scale over the EPIC-pn CCDs. This is mainly important for extended sources or sources away from the nominal aimpoint. For point sources close to the nominal aimpoint there should be little impact above ~ 1 keV, while at 0.6 keV, the reconstructed energy decreases by ~ 10 eV and thus decreases the tendency of overcorrection found at low energies (cf. Figs. 1, 2).

4 Estimated scientific quality

The scientific quality was estimated by the following technique: for extended sources with well–defined emission lines at sufficient statistics, the detector area was adaptively divided into regions containing a minimum number of photons around the emission line. This was done, separately for single and double pixel events, in detector coordinates, and the boundaries along the y–axis were aligned with the y ranges covered by the response matrices. The spectra extracted from each spectral region were fit with the response matrix corresponding to the particular region and pattern type, and the fit results were then projected back onto the corresponding CCD regions.

Figures 1 – 8 show maps of the spatial distribution of the energies derived in this way, colour coded according to the colour bar below, with the numbers referring to keV. The maps are displayed in detector coordinates, where the detector is seen from the direction of the telescope (i.e., these images are flipped with respect to those in sky coordinates). White boundaries mark the location of the 12 CCDs, in the sequence 3-2-1-4-5-6 from left to right in the top row, and 12-11-10-7-8-9 in the bottom row.

The sources which were investigated were Al–K and Mn–K from the internal calibration source in FF mode (rev 0080) and in eFF mode (revs 0532+0533), and the Vela SNR in FF mode, where exposures obtained from rev 0367 to 1635 were combined (after correcting for time dependent energy shifts between the individual observations) in order to get sufficient statistics. The Vela SNR was intentionally placed at various regions of the detector, in order to minimize any systematic effects due to changes of the intrinsic energies over the SNR, and in order to get a homogeneous irradiation of the detector.

In Figs. 1 – 8, the maps displayed at left show the energy distribution before running `epspatialcti`. In some of these maps (Figs. 1, 2, 3, 4, 7, 8), there is evidence for a dark ring accompanied by a dark band running horizontally through the middle. This structure results from the following effect: the electronic board behind the CCDs (as seen from the direction of the telescope) contains an opening which roughly corresponds to the inner area of the dark ring. Some infrared emission originating from the operation of the detector reaches the CCDs in this area and reduces the charge transfer losses due to partial saturation of traps. The CTI correction algorithm in SAS takes CTI variations between individual CCD columns into account and considers the energy dependence of the CTI individually for each column as well as CTI changes induced by precursors (if their energy exceeds the low energy threshold), but it does not consider CTI changes within a column. This leads to a systematic undercorrection and overcorrection of the charge transfer loss in certain regions. In addition to this effect caused by variable irradiation, there is also evidence for intrinsic CTI changes within some columns. These are the main reasons for any residual inhomogeneities of the absolute energy scale which remain after the corrections applied in the SAS.

As a correct treatment of these inhomogeneities would require substantial modifications of the CTI correction algorithm, a simpler method was chosen, where an energy shift is added to the PI values of the final event list, when necessary. This treatment appears justified in view of the small amount of the correction (typically a few eV, corresponding to $\sim 1\%$ or less) and that in this way also inhomogeneities which are not directly caused by CTI effects can be empirically corrected. The energy shift is determined individually for each pixel and PI value. In the current CCF, this shift is

independent of the pattern type (single, double, ..) and the readout mode (FF, eFF).

The effect of the energy correction obtained with `epspatialcti` is illustrated in Fig. 1 – 8. It is evident that a suppression of the inhomogeneities can be reached. The amount of suppression can be quantified by computing the standard deviation of the energies which were derived for the individual areas. For a correct interpretation of this value, however, the statistical error in the energy distribution for each area has to be considered; otherwise even in the absence of any spatial inhomogeneities a non zero value would result. The standard deviations which were obtained after quadratically subtracting the statistical error are summarized in Table 1 and 2.

	0.6 keV	1.5 keV	5.9 keV
FF singles	5.6 → 5.4	5.4 → 4.4	6.8 → 5.3
eFF singles		8.3 → 7.5	14.2 → 13.0
FF doubles		6.9 → 5.5	14.9 → 14.5

Table 1: Standard deviation $\sigma_{\rm before} \rightarrow \sigma_{\rm after}$ (in eV) of the energies which were determined in the individual fields, after quadratically subtracting the statistical error, before and after running `epspatialcti`.

	0.6 keV	1.5 keV	5.9 keV
FF singles	4% (Fig. 1,2)	9% (Fig. 3)	12% (Fig. 4)
eFF singles		10% (Fig. 5)	8% (Fig. 6)
FF doubles		20% (Fig. 7)	3% (Fig. 8)

Table 2: Improvement of the spatial homogeneity of the absolute energy scale, determined by $1-\sigma_{\rm after}/\sigma_{\rm before}$.

These values were derived from in–orbit exposures, using the Vela SNR (O VII emission) and the internal Fe^{55} calibration source (fluorescence of Al–K and Mn–K). While the irradiation is fairly homogeneous in the case of the Vela SNR, this is less the case for Al–K and especially for Mn–K. The variable degree of inhomogeneous irradiation has to be taken into account when a comparison between the individual energies is made. In some cases the improvements expressed in Tab. 2 are small. Consequently, only a minor increase is expected in the overall energy resolution of diffuse X–ray emission which is extended over the full field of view. However, for spatially resolved spectra, like those of point–like sources located at various positions on the detector or of specific regions in SNRs or in galaxy clusters, the improvement is likely to be higher.

While an application of `epspatialcti` is straightforward and fast, the derivation of the CCF data is quite challenging and most demanding in terms of statistical quality, which must be sufficient to determine the energy with an accuracy of a few eV for each pixel. Only four data sets were found to meet these criteria. They were obtained in ground calibration flatfield exposures at Ge–L (1.2 keV), Fe–K (6.4 keV), Cu–K (8.0 keV), and Ge–K (9.9 keV) in the full frame (FF) mode. Correction values for other energies had to be derived by interpolation or (below 1.2 keV) by extrapolation. This is probably the main reason why the improvement at 0.6 keV is only about half of that at 1.5 keV and 5.9 keV (Tab. 2).

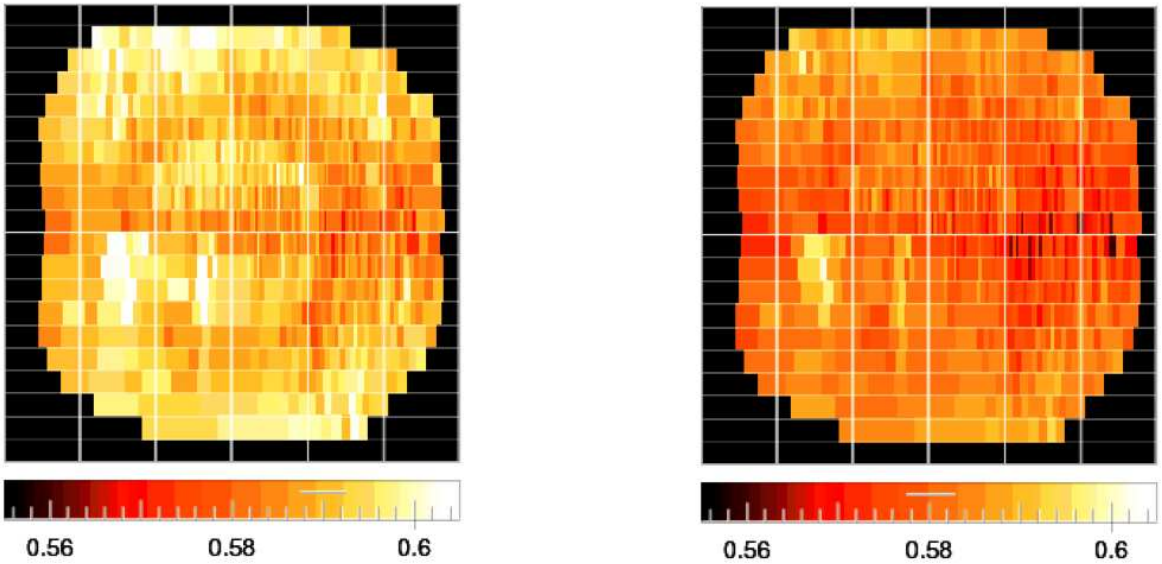

Figure 1: Comparison of the spatially resolved energy determination of the O VII line complex (nominal energy ≈ 0.574 keV) for singles in full frame mode, before (left) and after (right) running `epspatialcti`, displayed in the same colour coding. The statistical 1σ error in the energy determination is ± 2.6 eV for each area. The individual energy determinations exhibit a standard deviation of ± 6.2 eV before running epspatialcti and ± 6.0 eV afterwards. Taking the statistical uncertainties into account, this corresponds to a standard deviation of ± 5.6 eV before and ± 5.4 eV afterwards.

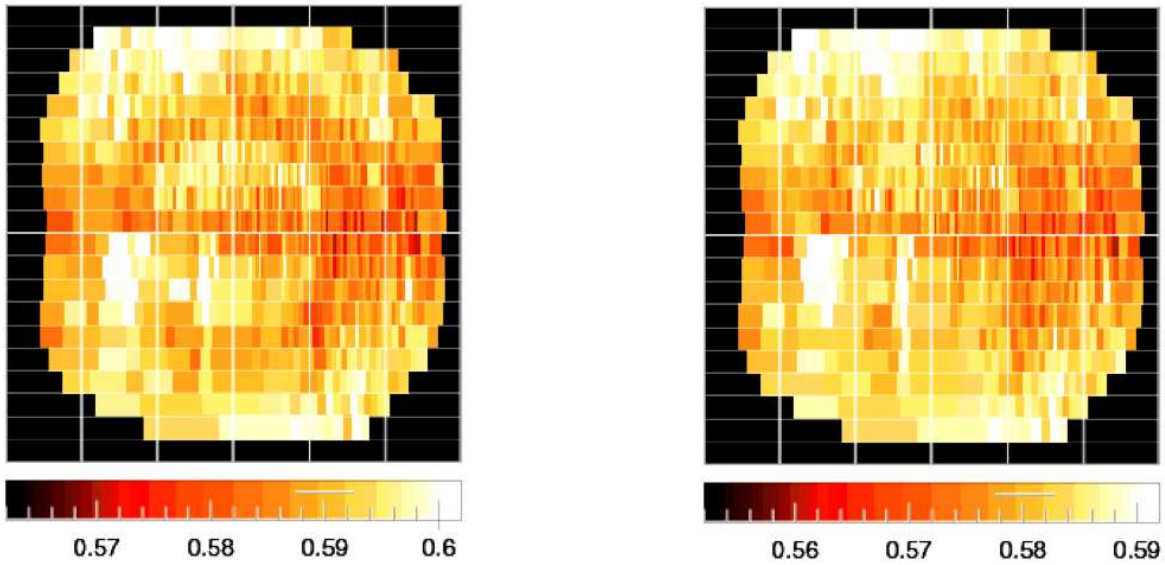

Figure 2: Same as Fig. 1, but displayed in enhanced contrast. In both cases, the colour code covers 40 eV, but extends from $0.562 - 0.602$ keV at left and from $0.552 - 0.592$ keV at right, in order to take the general decrease of the reconstructed energy by ~ 10 eV into account.

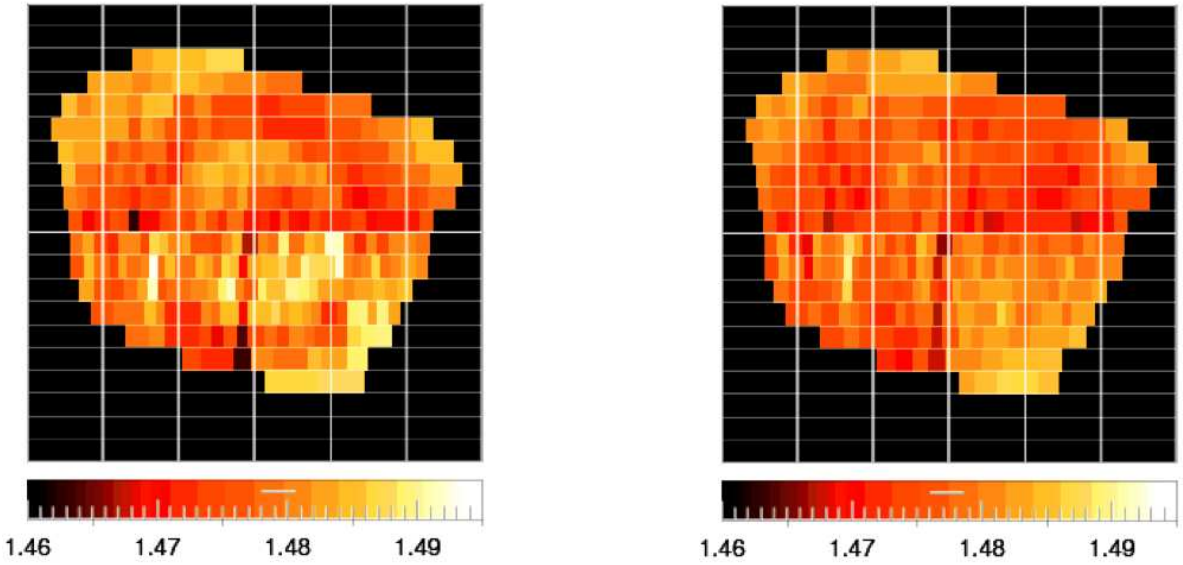

Figure 3: Comparison of the spatially resolved energy determination of the Al–K line (nominal energy 1.486 keV) for singles in full frame mode, before (left) and after (right) running `epspatialcti`, displayed in the same colour coding. The statistical 1σ error in the energy determination is ± 1.3 eV for each area. The individual energy determinations exhibit a standard deviation of ± 5.6 eV before running epspatialcti and ± 4.6 eV afterwards. Taking the statistical uncertainties into account, this corresponds to a standard deviation of ± 5.4 eV before and ± 4.4 eV afterwards.

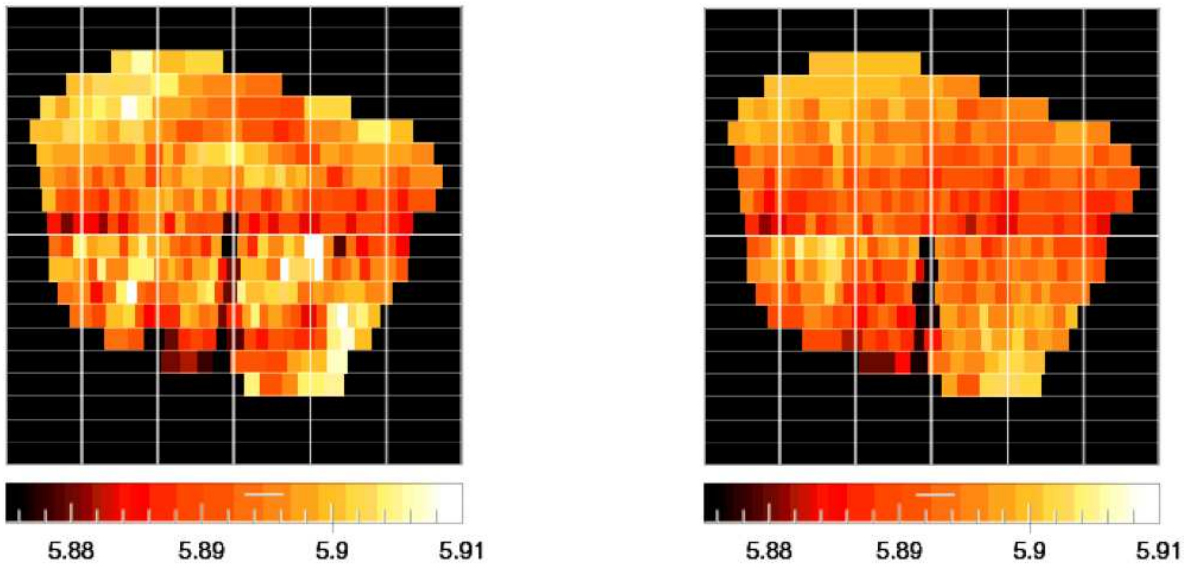

Figure 4: Comparison of the spatially resolved energy determination of the Mn–K_α line (nominal energy 5.896 keV) for singles in full frame mode, before (left) and after (right) running `epspatialcti`, displayed in the same colour coding. The statistical 1σ error in the energy determination is ± 1.5 eV for each area. The individual energy determinations exhibit a standard deviation of ± 7.0 eV before running epspatialcti and ± 5.5 eV afterwards. Taking the statistical uncertainties into account, this corresponds to a standard deviation of ± 6.8 eV before and ± 5.3 eV afterwards.

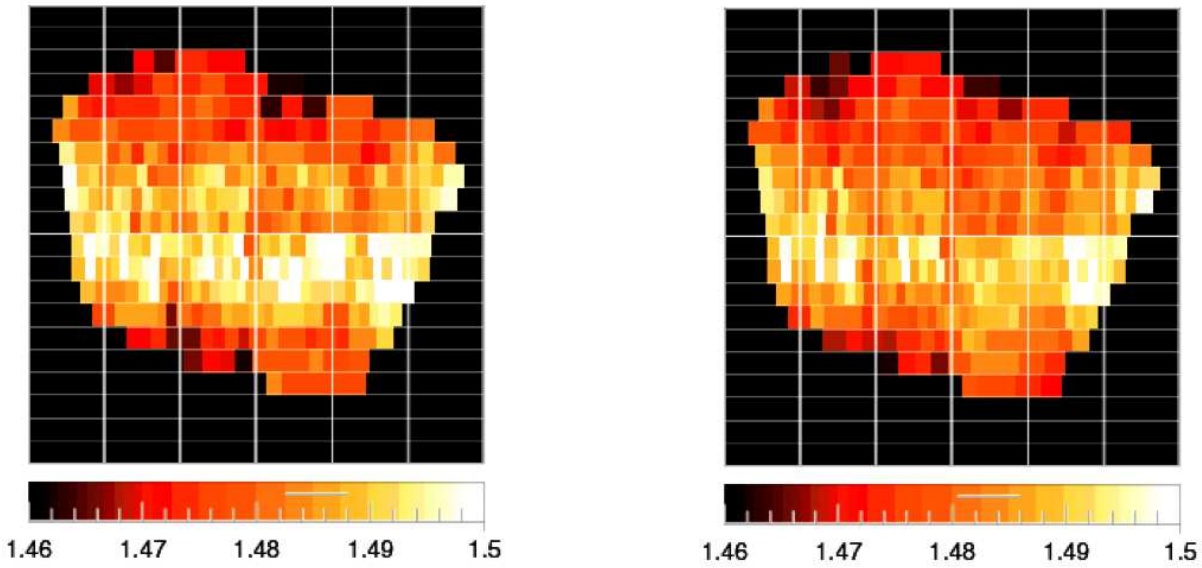

Figure 5: Comparison of the spatially resolved energy determination of the Al–K line (nominal energy 1.486 keV) for singles in extended full frame mode, before (left) and after (right) running `epspatialcti`, displayed in the same colour coding. The statistical 1σ error in the energy determination is $\pm$2.8 eV for each area. The individual energy determinations exhibit a standard deviation of $\pm$8.8 eV before running epspatialcti and $\pm$8.0 eV afterwards. Taking the statistical uncertainties into account, this corresponds to a standard deviation of $\pm$8.3 eV before and $\pm$7.5 eV afterwards.

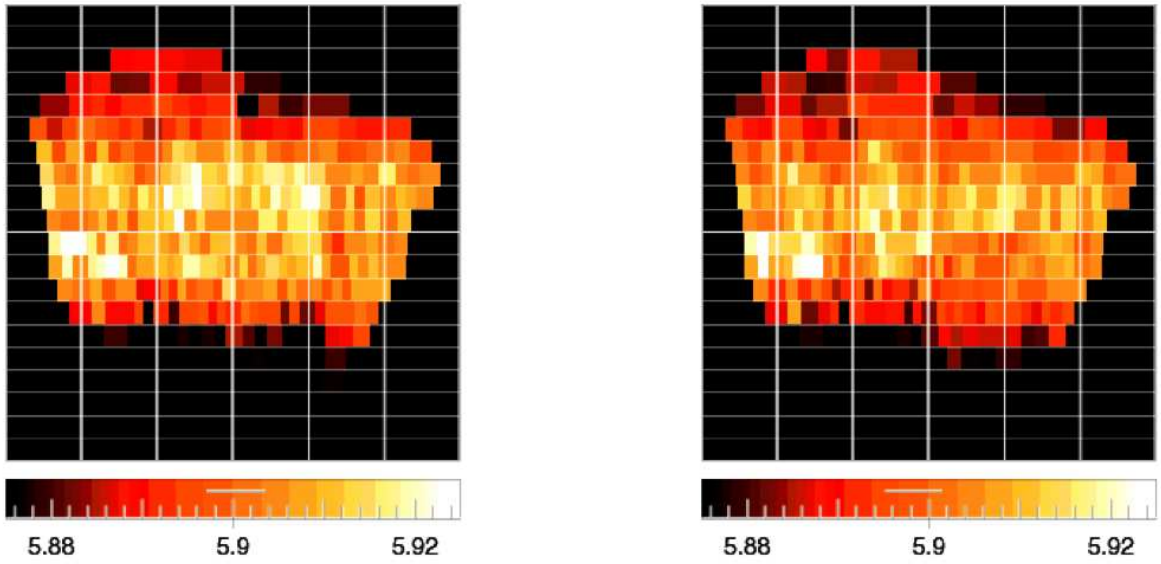

Figure 6: Comparison of the spatially resolved energy determination of the Mn–K_α line (nominal energy 5.896 keV) for singles in extended full frame mode, before (left) and after (right) running `epspatialcti`, displayed in the same colour coding. The statistical 1σ error in the energy determination is $\pm$3.2 eV for each area. The individual energy determinations exhibit a standard deviation of $\pm$14.6 eV before running epspatialcti and $\pm$13.4 eV afterwards. Taking the statistical uncertainties into account, this corresponds to a standard deviation of $\pm$14.2 eV before and $\pm$13.0 eV afterwards.

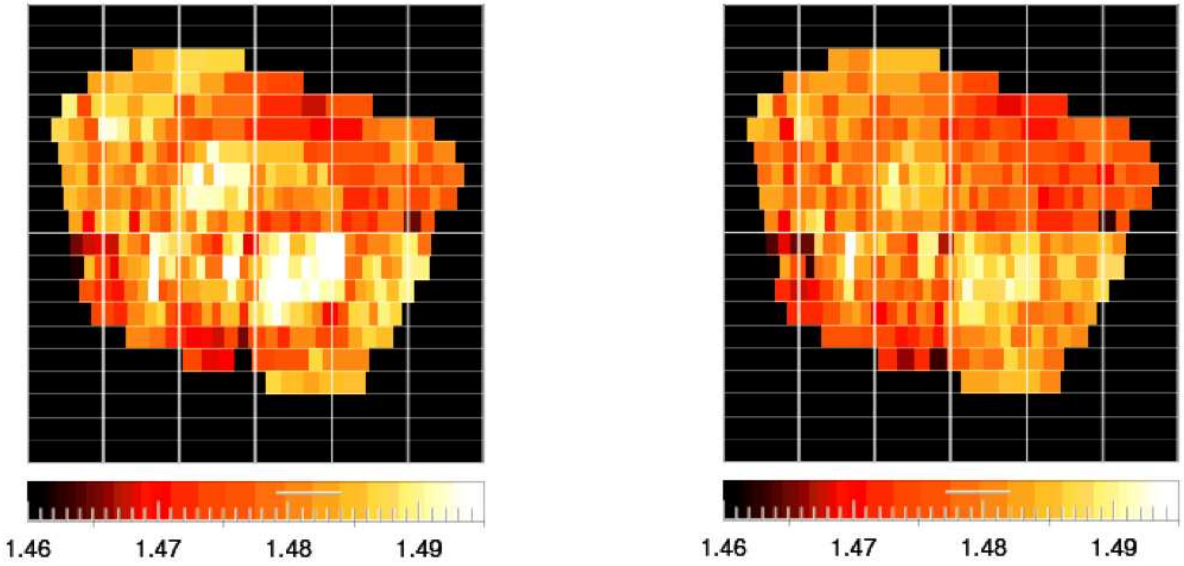

Figure 7: Comparison of the spatially resolved energy determination of the Al–K line (nominal energy 1.486 keV) for doubles in full frame mode, before (left) and after (right) running `epspatialcti`, displayed in the same colour coding. The statistical 1σ error in the energy determination is ± 2.5 eV for each area. The individual energy determinations exhibit a standard deviation of ± 7.3 eV before running epspatialcti and ± 6.0 eV afterwards. Taking the statistical uncertainties into account, this corresponds to a standard deviation of ± 6.9 eV before and ± 5.5 eV afterwards.

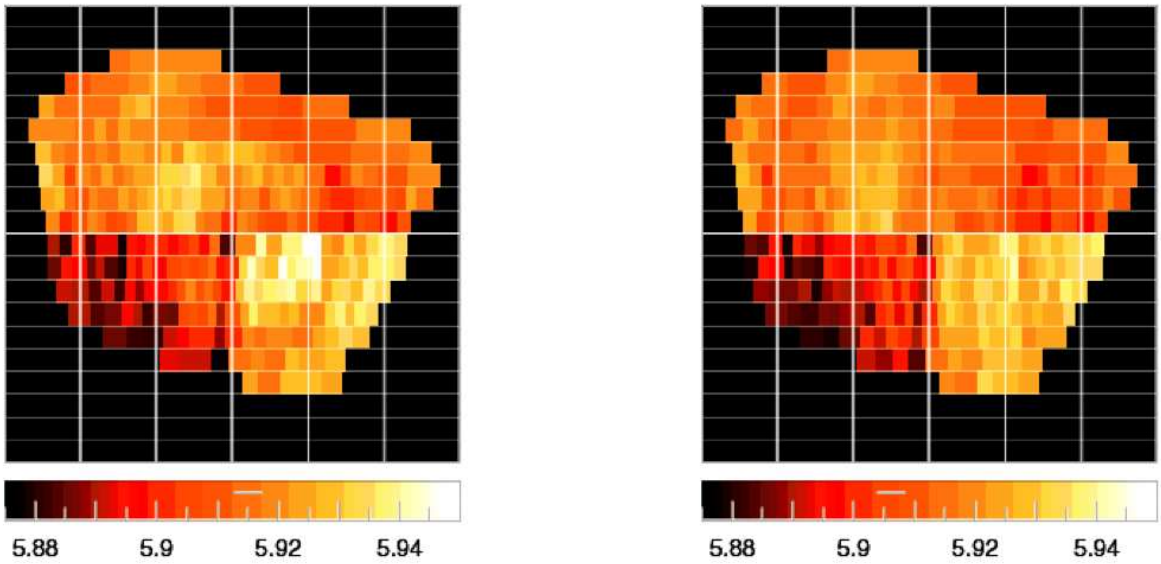

Figure 8: Comparison of the spatially resolved energy determination of the Mn–K_α line (nominal energy 5.896 keV) for doubles in full frame mode, before (left) and after (right) running `epspatialcti`, displayed in the same colour coding. The statistical 1σ error in the energy determination is ± 2.3 eV for each area. The individual energy determinations exhibit a standard deviation of ± 15.1 eV before running epspatialcti and ± 14.2 eV afterwards. Taking the statistical uncertainties into account, this corresponds to a standard deviation of ± 14.9 eV before and ± 14.0 eV afterwards.

5 Test procedure and results

Spectra were produced by extracting data from a circle of 5 arcminute radius about the Vela supernova. Data from 9 independent observations were combined into a single spectrum to improve statistics. The central energy of the lowest-energy component of the O VII triplet, fit by `XSPEC`, is originally found to be 566.5 ± 2.5 but changes to 562 ± 1 eV after `epspatialcti` is run on the individual event lists. The latter measurement is now consistent with the value of 561 eV expected from atomic physics.

6 References